

Novel methods for the synthesis of magnetite nanoparticles with special morphologies and textured assemblages

Ilona Nyiró-Kósa · Aleksander Rečnik ·
Mihály Pósfai

Received: 2 December 2011 / Accepted: 23 August 2012 / Published online: 26 September 2012
© Springer Science+Business Media B.V. 2012

Abstract There is an increasing technological demand for magnetic nanocrystals with special morphologies and controlled sizes. Several approaches are used for the synthesis of magnetite crystals with irregular or octahedral shapes; however, the room-temperature synthesis of nanocrystals with specific morphologies is not yet established. Here, we describe the synthesis of magnetite crystals (100–300 nm) at a relatively low temperature (~ 70 °C) from organic precursors, including Fe(II) oxalate or Fe(II) sulfate, and study the effects of ethylene glycol and tetraethylene glycol on the final physical and chemical properties of the crystals. The magnetite crystals formed from different precursor materials (sulfate or oxalate green rust) show specific morphological and textural features. We show that octahedral magnetite crystals can be produced from Fe(II) oxalate via a simple co-precipitation process. Using different kinds and amounts of polyols, various types of particle

morphologies and nanocrystal textures can be produced, including hexagonal-shaped clusters of elongated crystals and porous and solid, large, rounded polycrystalline aggregates.

Keywords Magnetite · Special morphology · Low-temperature precipitation · Transmission electron microscopy

Introduction

Controlling the sizes, shapes, and compositions of magnetite nanoparticles has become an important issue because of the technological applications that require magnetic nanoparticles with specific physical properties (Asmatulu et al. 2005; Gupta and Gupta 2005; Zahn 2001; An et al. 2006). There are several methods for synthesizing euhedral or irregularly shaped magnetite nanoparticles with sizes from ~ 5 to 120 nm, including co-precipitation, hydrothermal and electrochemical synthesis, ultrasound irradiation, and pyrolysis. However, many applications need magnetic nanoparticles that have special (elongated or rounded) shapes and carefully controlled, narrow size distributions (Corr et al. 2008; Liu et al. 2005). For example, μm -sized spherical magnetic particles were used in magnetic resonance imaging (MRI) fluid formulations and hollow and porous particles were suggested as drug

I. Nyiró-Kósa (✉)
Department of Material Engineering, University
of Pannonia, Egyetem Street 10, Veszprém 8200, Hungary
e-mail: kosaili@gmail.com

A. Rečnik
Department for Nanostructured Materials, Jožef Stefan
Institute, Jamova cesta 39, 1000 Ljubljana, Slovenia

M. Pósfai
Department of Earth and Environmental Sciences,
University of Pannonia, Egyetem Street 10, Veszprém
8200, Hungary

carriers in medicine or as adsorbents in environmental engineering (Salata 2004; Wei et al. 2006). Macroscopic magnetite crystals of diverse shapes can be synthesized at relatively high pressure and temperature. For example, magnetite was produced by the reduction of hematite (Gaviria et al. 2007). Ellipsoidal polycrystalline magnetite particles were synthesized in a two-step conversion process of single hematite particles by reduction in a hydrogen atmosphere and subsequent reoxidation in air (Itoh and Sugimoto 2003). In our previous work, we investigated the effects of various synthesis conditions in low-temperature inorganic co-precipitation processes on the size and morphology of magnetite nanoparticles (Nyiró-Kósa et al. 2009).

Organic compounds, including iron(II) oxalate (humboldtine), are promising starting materials for the formation of various iron oxide nanoparticles. The decomposition of humboldtine was studied extensively. In air, the final decomposition product is hematite (α -Fe₂O₃), whereas under reducing conditions, either magnetite (Fe₃O₄) or elemental iron is produced, depending on the partial pressure of oxygen (Frost and Weier 2004). Thermal decomposition of humboldtine at 500 and 700 °C results in the formation of magnetite with crystallite sizes in the range of 35–55 nm if treated under reduced oxygen partial pressure (Angermann and Töpfer 2008). Alternatively, polyols such as ethylene glycol (EG) and tetraethylene glycol (TEG) can be used for the reduction of metal salts (Cai and Wan 2007). They serve as high-boiling solvents and reducing agents as well as stabilizers to control the growth of particles and prevent their aggregation. Hou et al. (2003) synthesized 8–11-nm-sized magnetite crystals by solvothermal reduction of iron(III)-acetylacetonate (Fe(acac)₃) using EG solution of hydrazine, polyvinyl pyrrolidone, and trioctylphosphine oxide or hexadecylamine. 20-nm-sized magnetite crystals were synthesized at 280 °C using Fe(acac)₃, EG, and its oligomers (Cai and Wan 2007). Most recently, low-temperature synthesis of magnetite nanoparticles in the presence of organic precursors started to emerge in the literature; for instance, magnetite nanoplates were synthesized by ultrasonic irradiation using sodium acetate at 80 °C (Cheng et al. 2011) and irregular magnetite crystals were synthesized in diethylene glycol at 90 °C (Srivastava et al. 2011).

Morphology, size control, and low production cost are major objectives in the synthesis of magnetite nanoparticles. In the present study, our aim was to find

easy and reproducible methods to produce magnetite crystals with unusual, spherical or elongated morphologies. We describe the synthesis of magnetite crystals at 70 °C from organic Fe(C₂O₄)·H₂O (humboldtine) and inorganic FeSO₄·7H₂O (melanterite) reagents using organic additives EG and TEG. Details of the organic co-precipitation process were investigated with an emphasis on their effects on the final physical properties (size and morphology) of the product.

Experimental procedures

Synthesis

Distilled water was used for the preparation of all solutions and for washing the magnetic precipitate after the synthesis. All solutions were deaerated with nitrogen in order to avoid the oxidizing effect of air, and a nitrogen-filled glove box was used during the reaction and aging process. The pH and the temperature of the solutions were measured during the synthesis (inoLab Level 3 pH meter, WTW GmbH, Weilheim, Germany). Depending on the starting materials, two sets of processes were distinguished, as marked by Roman numerals (Table 1). Reaction runs were assigned into subgroups according to the variable parameters of the reaction conditions.

Synthesis route I

1.35 g of FeC₂O₄·2H₂O (humboldtine) powder was mixed with 10 ml distilled water and magnetically stirred, while 12.5 ml 1.75 M NaNO₃ (as an oxidizing agent) and 25 ml 2 M NaOH alkaline solution were added. Because of the insolubility of humboldtine in water (0.22 g/100 g water, *T* = 25 °C), the oxidizing and the alkaline solutions were practically added to a water–crystal mixture. The yellow color of the ferrous oxalate powder turned into a greenish-blue color after NaOH addition. This material was then heated and aged at 70 °C for 2 h, when a black, magnetic precipitate was produced.

Synthesis route II.1

2.85 g FeSO₄, 4.25 g NaOH, and 0.5 g NaNO₃ were dissolved in 7.5, 25, and 12.5 ml, respectively, of 1:1

Table 1 Synthesis conditions and products

Sample	Reagent 1	Reagent 2	Reagent 3	T (°C)	PH	Reaction time (hours)	Solvent composition	Atmosphere	Products	Magnetite morphology	Mean size by TEM (nm)	Shape factor (width/length)	Cell parameter(A)
I.	FeC ₂ O ₄	NaNO ₃	NaOH	70	11	2		N ₂	Magnetite	Octahedral	100	0.9	8.397
II.													
1.	FeSO ₄	NaNO ₃	NaOH	70	12.3	24	TEG:H ₂ O = 1:1	N ₂	Magnetite	Elongated	ND	ND	8.376
2.	FeSO ₄	NaNO ₃	NaOH	70	12	24	TEG:H ₂ O = 3:1	N ₂	Magnetite	Rounded	62	0.9	8.377
3.	FeSO ₄	NaNO ₃	NaOH	70	12.3	2	EG:H ₂ O = 1:1	N ₂	Magnetite	Rounded	277	0.95	8.354

ND not determined

TEG/water solution and heated to 70 °C. After adding the NaOH to the FeSO₄ solution, a greenish-blue precipitate was produced, the color of which did not change after stirring for 2 h and aging it for a day under N₂ atmosphere. Because the pH of the solution was 4.5 after aging for a day, we added more NaOH to the precipitate to reach pH = 10 that is optimal for magnetite formation (Schwertmann and Cornell, Cornell and Schwertmann 2003). The precipitate was then stirred at 70 °C for additional 2 h, and finally a magnetic, black precipitate formed.

Synthesis route II.2

The above reaction was repeated in a 3:1 volume ratio TEG/water solution. The transformation from the greenish-blue precipitate into magnetite was achieved after 30-min stirring without the addition of extra NaOH. The product was aged for a day and the pH was stabilized with the addition of 5 ml 1 M NaOH and 5 ml TEG because of the low pH = 4.7 of the solution.

Synthesis route II.3

Reaction II.1 was repeated using EG instead of TEG. In this case a black, magnetic precipitate was produced after 2 h of aging of the intermediate product.

Product characterization

In order to examine the products, samples for transmission electron microscopy (TEM) and X-ray powder diffraction (XRD) measurements were taken from the greenish-blue precipitate as well as from the final product. For XRD analysis, two intermediate samples were filtered and dried in vacuum because of their sensitivity to oxygen. The oxalate sample oxidized rapidly during this sample preparation process, while the sulfate sample was stable. The stability of the sulfate samples is a result of TEG addition, which forms a hydrophilic polyol ligand coating that prevents further oxidation of the intermediate product. Precipitated magnetite particles were filtered and washed in deionized water in order to remove extraneous ions, and finally dried at room temperature. TEM samples of the intermediate and final products were prepared by depositing a drop of their suspension in ethanol onto Formvar-covered Cu grids.

Phase compositions were measured by an X-ray powder diffractometer (XRD; Philips PW 1710) operated at 50 kV and equipped with a graphite monochromator and a proportional detector. Unit cell refinement of magnetite was performed in the $Fd\bar{3}m$ space group for 1.5418 Å X-ray wavelength on using the average of two lines of Cu-K α radiation (Celref V3 software; Schmitt and Ouladdiaf 1998). At least six reflections were assigned manually for refinement. For a determination of the confidence interval, each sample was measured three times and the largest difference was taken as the error of the unit cell parameter. Crystal size distribution and morphology were studied by complementary TEM techniques (JEOL 3010 operated at 297 kV, Philips CM20 microscope operated at 200 kV, and a 200 kV JEOL 2100 TEM). Particle size measurements were done on the two-dimensional projections of grains in bright-field (BF) TEM images (ImageJ software). We obtained size distributions by fitting ellipses to the outlines of the crystals and used the average of the two axes as the diameter. About 150 particles were measured in each sample. For studying the morphologies of the products, we obtained BF TEM images. High-resolution (HRTEM) images were taken to measure lattice parameters and to study the crystal structures. Selected-area electron diffraction (SAED) patterns were obtained for crystal identification of individual particles and lattice parameter measurements.

Results

Intermediate products

A greenish-blue intermediate product formed in both synthesis routes. While in route I (using Fe(II) oxalate), the intermediate material was produced from yellow, crystalline oxalate phase, in route II (using FeSO₄ as the starting material), it precipitated from the FeSO₄ solution.

The intermediate phases were green rusts (GR) in all synthesis runs. These are double-layered hydroxysalts, consisting of positively charged Fe(II)/(III) hydroxide sheets that are intercalated with layers of water molecules and anions (Cornell and Schwertmann 2003). The general formula of green rusts can be given as $[\text{Fe(II)}_{1-x}\text{Fe(III)}_x(\text{OH})_2]^{x+} [(x/n)\text{A}^{n-}m\text{H}_2\text{O}]^x$. Depending on the type of the Aⁿ⁻ anions,

we distinguish two types of green rusts (GR-I and GR-II). GR-I contains chloride, carbonate, or oxalate anions and has a trigonal structure resembling that of pyroaurite (Refait et al. 1998). In GR-II, the intercalated Aⁿ⁻ anions are sulfate or selenate, and the structure is also trigonal, but with a much smaller periodicity (1.1 vs. 2.3 nm) along the *c*-axis (Legrand et al. 2004).

The morphologies of grains of the intermediate products were consistent with the well-known hexagonal morphologies of both GR-I and GR-II (Génin et al. 2002) as observed in the TEM. We assume that the intermediate product that formed from iron(II) oxalate is GR-I, although we could not obtain electron diffraction patterns from this material because of its extreme sensitivity to the electron beam. Grains of GR-I ranged in size between 200 and 800 nm and rapidly decomposed under the electron beam. The intermediate phase in synthesis route II was identified by XRD as sulfate green rust (GR-II) (Fig. 1). GR-II is more stable under the electron beam than GR-I. Its crystals have characteristic, platy hexagonal morphologies with a mean particle size of 340 nm.

Magnetite products

XRD analysis shows that all synthesis products are magnetite (Fig. 2). In sample II.1, minor goethite (14 %) appeared in addition to magnetite (86 %).

Nanocrystals precipitated from Fe(II) oxalate (synthesis route I) have a regular octahedral shape (Fig. 3) consistent with the equilibrium morphology of magnetite. The edges and corners of the crystals can be clearly seen in the bright-field images, indicating the well-defined crystal morphology even of the smallest crystals. The mean crystal size is 100 nm, and the size distribution is lognormal (Fig. 4a). In addition to sharp octahedral crystals, we observe thin rod-like crystals of goethite, which result from partial hydration of the product.

Synthesis route II.1 (Table 1) produced elongated, rod-shaped magnetite crystals. In many places on the TEM grid, the elongated crystals are arranged in clusters that have straight outlines and pseudo-hexagonal shapes, suggesting that a relict shape of the precursor crystals was preserved during the phase transformation (Fig. 5). The pseudo-hexagonal aggregates consist of radiating arrays of nanocrystals that are surrounded by a distinct solid rim. Electron diffraction

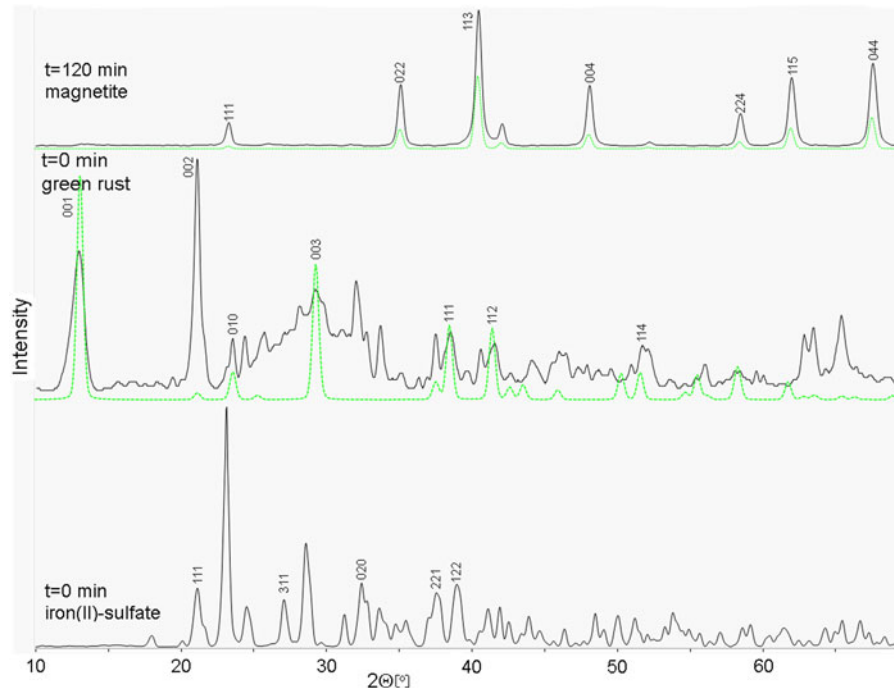
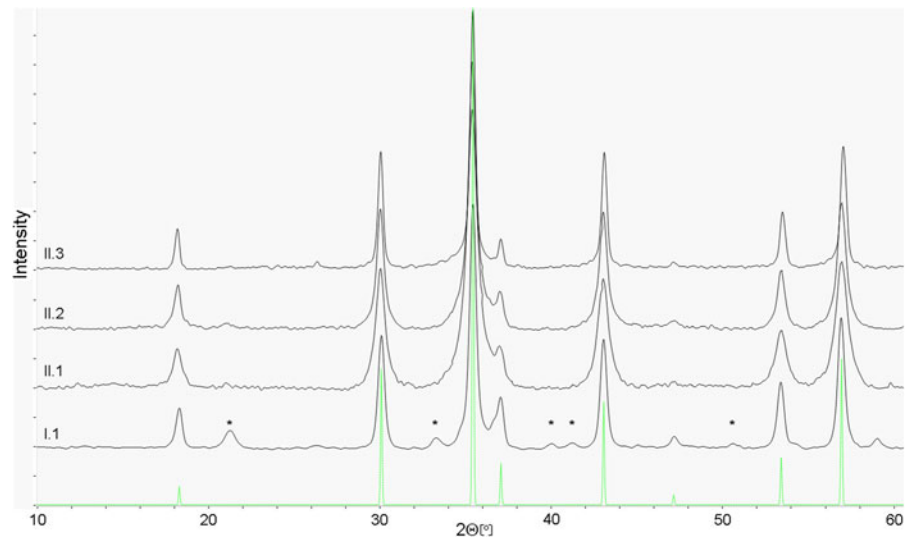


Fig. 1 XRD patterns of the starting material (Fe(II) sulfate), intermediate product (GR-II), and final product (magnetite) in synthesis route II.1. Larger background and small lines result

from TEG. *Dashed lines* indicate the positions of the XRD peaks of the pure compounds

Fig. 2 XRD patterns of all synthesis products. *Dashed lines* indicate the calculated positions of the peaks of pure magnetite. Goethite peaks are marked by *asterisks*



from larger areas shows reflections consistent with a spinel-type structure. The *d* values of all diffraction rings correspond to magnetite. At higher magnifications, we observe that both the rim and the radially oriented magnetite crystals within such a pseudomorphic assemblage have the $[1\bar{1}0]$ axis of magnetite

oriented parallel with the $[0001]$ axis of former GR-II crystals, and $[111]_{\text{magnetite}}$ is parallel with $[11\bar{2}0]_{\text{GR-II}}$. Individual magnetite crystals are elongated along different directions depending on the recrystallization paths within the former GR-II crystal. Here, we find aggregates of pseudo-octahedral crystals linked by

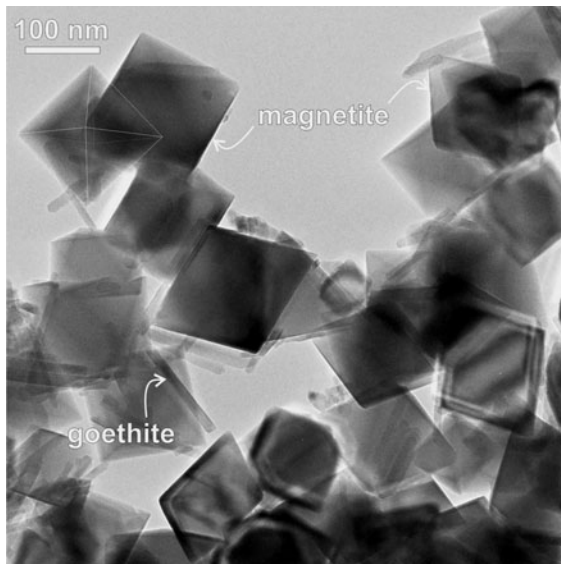


Fig. 3 Octahedral magnetite crystals with sharp edges produced in synthesis route I. The elongated crystals are goethite

their edges (Fig. 5b) or even long magnetite ribbons with large (111) faces if they grew along $[11\bar{2}]$ (Fig. 5c). Such ribbons are unusual for magnetite and they could only form because of selective growth directions during crystallization.

Magnetite particles produced in synthesis route II.2 are round with irregular outlines and produce a heterogeneous contrast in BF images as a result of their polycrystalline character (Fig. 6a). The particles consist of an ensemble of smaller crystals. However, SAED patterns obtained from these particles show a single-crystal orientation (Fig. 6b), implying that all magnetite nanocrystals within these aggregates have identical orientation. Magnetite aggregates have a porous structure. The size distribution of the particles

is bimodal (Fig. 4b) with mean sizes of 62 nm for the aggregates and 7 nm for magnetite nanocrystal subunits.

Crystals from synthesis route II.3 have similar morphologies and similar sizes to those from synthesis route II.2. However, they do not contain pores. Most of the particles show uniform contrast in TEM images without a gradual change from the edge to the center of the particle, indicating a constant thickness and a disk-shaped morphology (Fig. 7). Other particles display heterogeneous, sectorial contrast changes as a result of diffraction effects. We assume that this contrast variation is caused by slight misorientation of the parts relative to one another, probably resulting from the coalescent growth of the particles. HRTEM images show that the particles with a uniform contrast are composed of magnetite nanocrystals that have a consensus orientation (A and B insets in Fig. 7a). This is supported by a single-crystal SAED pattern recorded from a large particle. This particle is in $[114]$ orientation based on the SAED pattern (Fig. 7b). The mean size of the magnetite crystals is 277 nm (Fig. 7c). In this sample, the unit cell parameter (Table 1) is slightly smaller than for the other three samples. This can be caused by partial maghemitization of this sample.

Discussion

In the present study, magnetite crystals with different morphologies were produced using organic compounds either as starting materials or as media for coprecipitation processes. All magnetite samples formed from various green rust intermediate products. Since

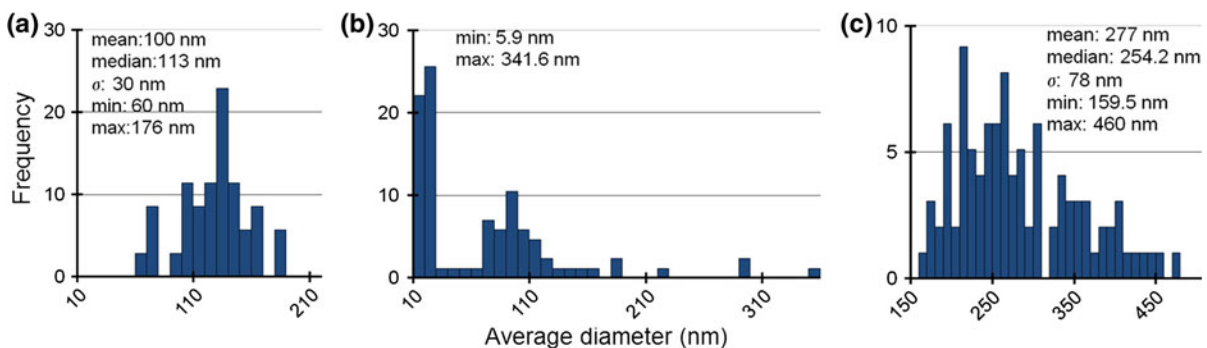


Fig. 4 Crystal size distributions of magnetite nanoparticles from synthesis routes I (a), II.2 (b), and II.3 (c)

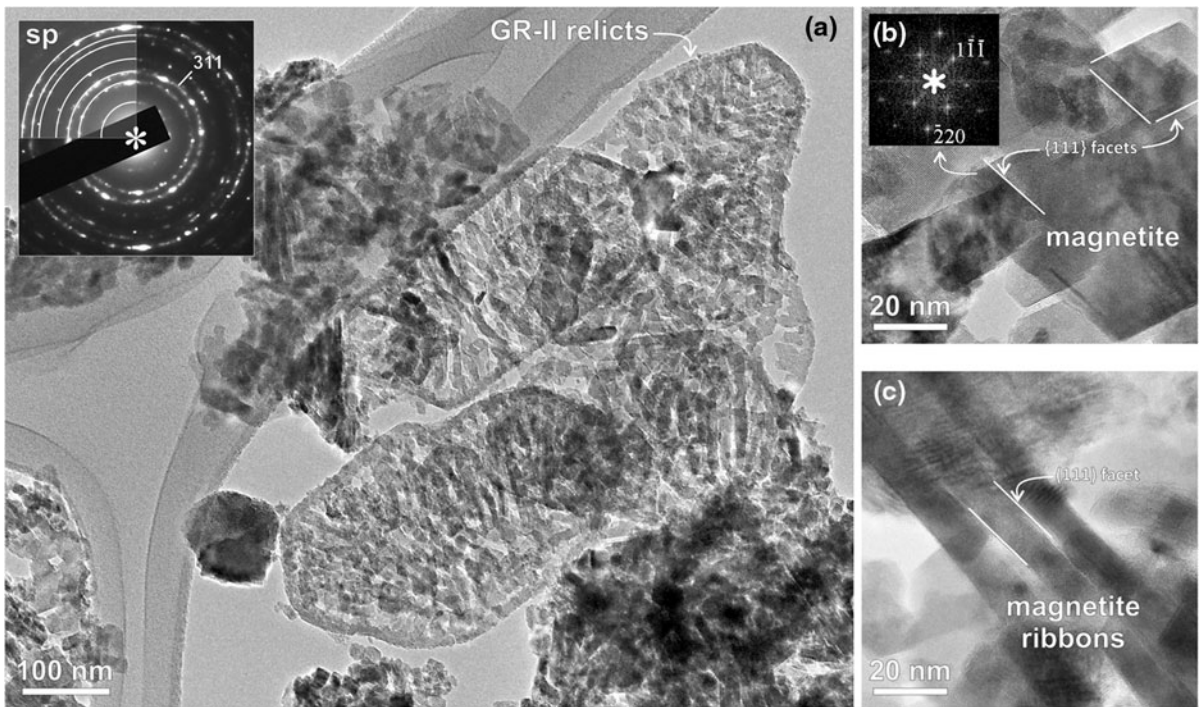


Fig. 5 Pseudo-hexagonal magnetite aggregates produced in synthesis route II.1. **a** Highly porous aggregates are composed of interconnected, lath-shaped magnetite nanocrystals, which maintained an orientation relationship with the precursor GR-II crystals. Electron diffraction pattern taken from a larger area

corresponds to magnetite (sp: calculated rings; all observed rings correspond to magnetite and no magnetite ring is missing). **b** HRTEM image of laterally connected euohedral magnetite crystals and **c** detail of magnetite ribbons with extended (111) facets

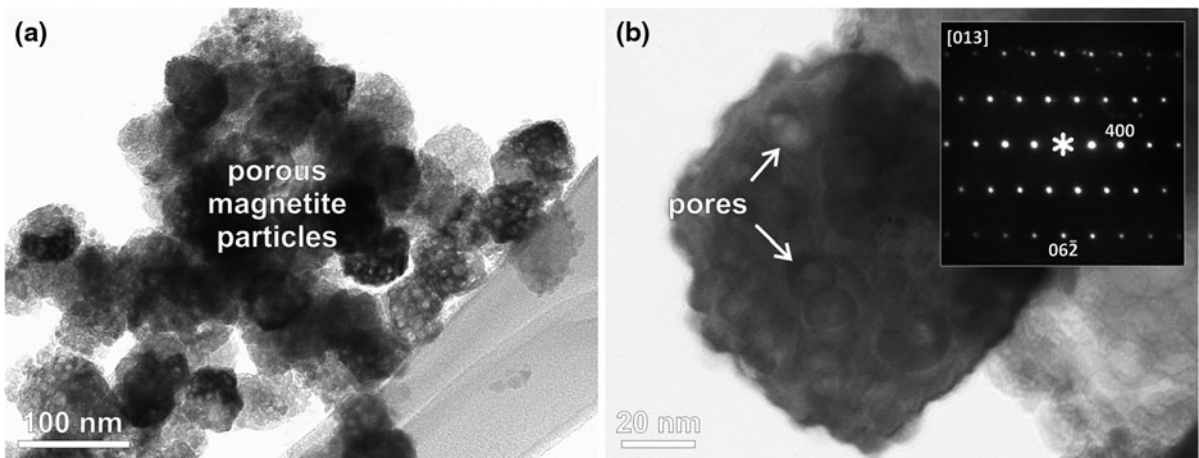


Fig. 6 a Particles in sample II.2 have wavy outlines and a heterogeneous contrast, some of which is a result of electron-beam damage. **b** A round, porous particle in sample II.2. The

inserted electron diffraction pattern indicates that the particle is a single magnetite crystal in [013] orientation

the starting material was iron oxalate in synthesis I, we assume that the intermediate product was oxalate green rust (GR-I). This assumption is supported by the

results of Refait et al. (1998) who synthesized Fe(II)-Fe(III) hydroxy oxalate green rust by oxidation of Fe(II) hydroxide that was precipitated from Fe(II)

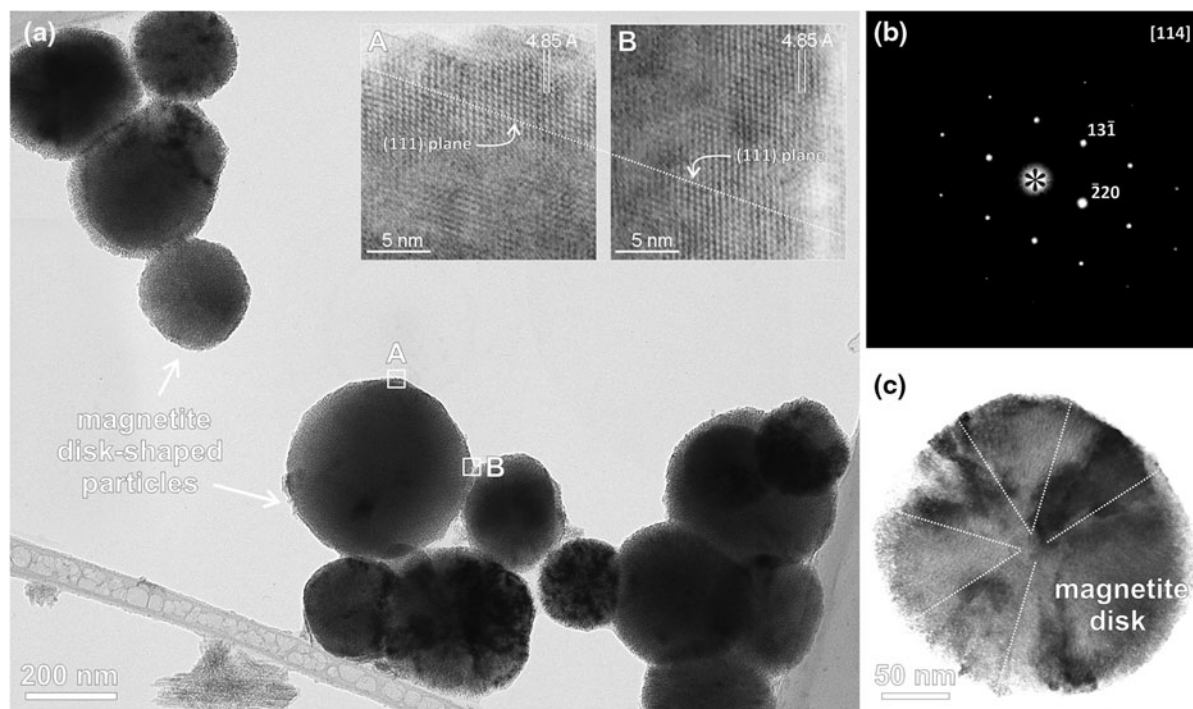


Fig. 7 **a** Round-shaped magnetite crystals from synthesis II.3. The particles consist of many small crystallites that have a consensus orientation (A and B) and thus produce a single-

crystal diffraction pattern **(b)** taken along the [114] zone axis. **c** The particle shows sectorial contrast

oxalate and NaOH. In the reactions that used iron sulfate (syntheses route II), we identified the intermediate product as hydroxysulfate green rust (GR-II) that formed hexagonal-shaped platelets with a mean size of 340 nm and a thickness of ~ 24 nm. The GR-I sample was rapidly oxidized during the sample preparation process, while GR-II was stable owing to the TEG additive.

While synthesis route I produced nanocrystals with the equilibrium, octahedral, morphology of magnetite, the addition of EG and TEG to the solution resulted in unusual crystal morphologies. Magnetite crystals synthesized in a 1:1 mixture of TEG and water are elongated and arranged in hexagonal-shaped clusters. This special texture is due to the shape of the precursor crystal from which the magnetite crystals transformed. The conversion of GR-II to magnetite in an aqueous medium was studied by Sumoondur et al. (2008), who suggested a mechanism involving dissolution/recrystallization processes. Their intermediate product was a stable phase at neutral and low pH, which is consistent with a pH of 4 in our case. The addition of an alkaline solution increased the pH and caused the formation of

magnetite. During the recrystallization process, the volume could change, resulting in the open, porous structure of the pseudo-hexagonal magnetite aggregates.

Magnetite particles synthesized in a 3:1 mixture of TEG and water are round shaped with a heterogeneous TEM contrast that indicates some degree of porosity. Particles synthesized in a 1:1 EG and water mixture are also round shaped, but formed from an intermediate product without the addition of an alkaline solution. Both magnetite products are polycrystalline. The nanocrystals are attached to one another in a uniform orientation; thus, the polycrystalline particles with diameters of tens to several hundred nm produce single-crystal diffraction patterns. Our results are similar to those obtained by Yu et al. (2006) who synthesized 200–400-nm-sized hollow microspheres at 220 °C using EG and dodecylamine (DDA). A change of DDA concentration played an important role in the formation of either hollow or solid microspheres, and in both cases, the crystallites within such spheres had identical orientation, similar to that observed in our samples.

The growth mechanism of primary iron oxide nanoparticles in aqueous solutions has been a subject of several studies (Blesa and Matijevic 1989; Combes et al. 1990). Based on these results, the hydroxyl groups play a major role in the aggregation of metal oxide nanoparticles. However, little information is available on the mode of attachment in non-aqueous, organic solutions. Water appeared to be an essential ingredient for the aggregation of Co_3O_4 nanocrystals that were synthesized in n-hexanol (He et al. 2004). The aggregation of crystals is slower in non-aqueous than in aqueous solutions because of a higher viscosity and fewer surface hydroxyl groups. Thus, the nanocrystals are able to arrange in a form that produces the lowest surface energy by developing a perfectly oriented attachment. The individual magnetite crystals arrange with such perfection that they produce a diffraction pattern characteristic of a single crystal. Finally, the coalescence of the attached particle clusters results in the formation of a single crystal. In our case, the intermediate crystal (without coalescence) can be seen in synthesis route II.2 (Fig. 6b), where the islands of little crystals are clearly seen in particles with heterogeneous contrast. The individual crystals in disk-shaped aggregates from the synthesis route II.3 (Fig. 7a) are merged as a result of radial coalescent growth of magnetite crystals.

In summary, we showed that uniform octahedral magnetite crystals can be produced from humboldtine at a low temperature by a simple precipitation process. Magnetite with an octahedral shape could also be produced in an aqueous medium using iron sulfate as the starting material (Nyiró-Kósa et al. 2009); however, the same reaction in organic/water media resulted in crystals with non-equilibrium morphologies. Particles synthesized in the presence of TEG are elongated and arranged in hexagonal-shaped clusters. By varying the TEG/water ratio, we produced large particles with either porous or compact structures that consist of smaller crystallites in a consensus orientation. All proposed synthesis methods are non-toxic, low cost and easily reproducible. The magnetite products described in this study could find potentially interesting technological applications. For example, the perfect octahedra could be used in magnetic storage, whereas porous microspheres and large disk-shaped particles could be implemented in medical applications as carriers of active ingredients due to their special hollow structure and hydrophilic properties. Due to

their large surface area, some of our products could also be used in wastewater treatment as absorbent bases that can be magnetically separated.

Acknowledgments This study was supported by an intergovernmental Hungarian-Slovenian grant for bilateral research cooperation (TÉT-SI-10/2008) and an EU FP7 grant (BIO2MAN4MRI). Ilona Nyiró-Kósa benefited from the ESF Research Training Network program FIMIN. The authors acknowledge the microscopy work support from the Research Institute for Technical Physics and Materials Science, Budapest, Hungary and the Jožef Stefan Institute, Ljubljana, Slovenia.

References

- An L, Li ZQ, Li W, Nie YR, Chen ZM, Wang YP, Yang B (2006) Patterned magnetite films prepared via soft lithography and thermal decomposition. *J Magn Mag Mat* 303:127–130
- Angermann A, Töpfer J (2008) Synthesis of magnetite nanoparticles by thermal decomposition of ferrous oxalate dihydrate. *J Mat Sci* 43:5123–5130
- Asmatulu R, Zalich MA, Claus RO, Riffle JS (2005) Synthesis, characterization and targeting of biodegradable magnetic nanocomposite particles by external magnetic fields. *J Magn Mag Mat* 292:108–119
- Blesa MA, Matijevic E (1989) Phase transformation of iron-oxides, oxohydroxides, and hydrous-oxides in aqueous media. *Adv Coll Interf Sci* 29:173–221
- Cai W, Wan J (2007) Facile synthesis of superparamagnetic nanoparticles in liquid polyols. *J Colloid Interface Sci* 305:366–370
- Cheng JP, Ma R, Shi D, Liu F, Zhang XB (2011) Rapid growth of magnetite nanoplates by ultrasonic irradiation at low temperature. *Ultrason Sonochem* 18:1038–1042
- Combes JM, Manceau A, Calas G (1990) Formation of ferric oxides from aqueous solutions: A polyhedral approach by X-ray Absorption Spectroscopy: II Hematite formation from ferric gels *Geochim Cosmochim Acta* 54:1083–1091
- Cornell RM, Schwertmann U (2003) *The iron oxides*. Wiley, Weinheim, p 530
- Corr SA, Rakovich YP, Gun'ko YK (2008) Multifunctional magnetic-fluorescent nanocomposites for biomedical application. *Nanoscale Res Lett* 3:87–104
- Frost RL, Weier ML (2004) Thermal decomposition of humboldtine – a high resolution thermogravimetric and hot stage Raman spectroscopic study. *J Therm Anal Calorim* 75:277–291
- Gaviria JP, Bohe A, Pasquevich A, Pasquevich DM (2007) Hematite to magnetite reduction monitored by Mössbauer spectroscopy and X-ray diffraction. *Phys B* 389:198–201
- Génin A, Ruby C, Abdelmoula M, Benali O, Ghanbaja J, Refait P, Génin J-MR (2002) Synthesis of Fe(II-III) hydroxysulfate green rust by coprecipitation. *Solid State Sci* 4:61–66
- Gupta AK, Gupta M (2005) Synthesis and surface engineering of iron oxide nanoparticles for biomedical applications. *Biomaterials* 26:3995–4021
- He T, Chen D, Jiao X, Xu Y, Gu Y (2004) Surfactant-assisted solvothermal synthesis of Co_3O_4 hollow spheres with

- oriented-aggregation nanostructures and tunable particle size. *Langmuir* 20:8404–8408
- Hou YL, Yu JF, Gao S (2003) Solvothermal reduction synthesis and characterization of superparamagnetic magnetite nanoparticles. *J Mat Chem* 13:1983–1987
- Itoh H, Sugimoto T (2003) Systematic control of size, shape, structure, and magnetic properties of uniform magnetite and maghemite particles. *J Colloid Interf Sci* 265:283–295
- Legrand L, Mazerolles L, Chaussé A (2004) The oxidation of carbonate green rust into ferric phases solid state reaction or transformation via solution. *Geochim Cosmochim Acta* 68:3497–3507
- Liu F, Cao P, Zhang H, Tian J, Xiao C, Shen C, Li J, Gao H (2005) Novel nanopyramid arrays of magnetite. *Adv Mater* 17:1893–1897
- Nyirő-Kósa I, Csákberényi-Nagy D, Pósfai M (2009) Size and shape control of precipitated magnetite nanoparticles. *Eur J Mineral* 21:293–302
- Refait P, Charton A, Génin J-MR (1998) Identification, composition, thermodynamic and structural properties of a pyroaurite-like iron(II)-iron(III) hydroxy-oxalate green rust. *Eur J Solid State Inorg Chem* 35:655–666
- Salata O (2004) Applications of nanoparticles in biology and medicine. *J Nanobiotechnology* 2:3
- Schmitt D, Ouladdiaf B (1998) Absorption correction for annual cylindrical samples in powder neutron diffraction. *J Appl Cryst* 31:620–624
- Srivastava S, Awasthi R, Gajbhiye NS, Agarwal V, Singh A, Yadav A, Gupta RK (2011) Innovative synthesis of citrate-coated superparamagnetic Fe₃O₄ nanoparticles and its preliminary applications. *J Colloid Interf Sci* 359:104–111
- Sumoondur A, Shaw S, Ahmed I, Benning LG (2008) Green rust as a precursor for magnetite: an in situ synchrotron based study. *Min Mag* 72:201–204
- Wei X, Roger C, Viadero Jr (2006) Synthesis of magnetite nanoparticles with ferric iron recovered from acid mine drainage: implications for environmental engineering. *Colloid Surface A* 294:280–286
- Yu D, Sun X, Zou J, Wang Z, Wang F, Tang K (2006) Oriented assembly of Fe₃O₄ nanoparticles into monodisperse hollow single-crystal microspheres. *J Phys Chem B* 110:21667–21671
- Zahn M (2001) Magnetic fluid and nanoparticle applications to nanotechnology. *J Nanopart Res* 3:73–78